Alginate Gel-Mediated Photochemical Growth of Mono- and Bimetallic Gold and Silver Nanoclusters and Their Application to Surface-Enhanced Raman Scattering

ARTICLE *in* THE JOURNAL OF PHYSICAL CHEMISTRY C · APRIL 2009

Impact Factor: 4.77 · DOI: 10.1021/jp811235m

6 AUTHORS, INCLUDING:

Sandip Saha
National Sun Yat-sen University
21 PUBLICATIONS **491** CITATIONS
SEE PROFILE

Anjali Pal
IIT Kharagpur
140 PUBLICATIONS **4,311** CITATIONS
SEE PROFILE

Surojit Pande
Birla Institute of Technology and Science P…
45 PUBLICATIONS **1,628** CITATIONS
SEE PROFILE

Tarasankar Pal
IIT Kharagpur
254 PUBLICATIONS **8,733** CITATIONS
SEE PROFILE

THE JOURNAL OF PHYSICAL CHEMISTRY C

Article

Alginate Gel-Mediated Photochemical Growth of Mono- and Bimetallic Gold and Silver Nanoclusters and Their Application to Surface-Enhanced Raman Scattering

Sandip Saha, Anjali Pal, Surojit Pande, Sougata Sarkar, Sudipa Panigrahi, and Tarasankar Pal

J. Phys. Chem. C, **2009**, 113 (18), 7553-7560• DOI: 10.1021/jp811235m • Publication Date (Web): 14 April 2009

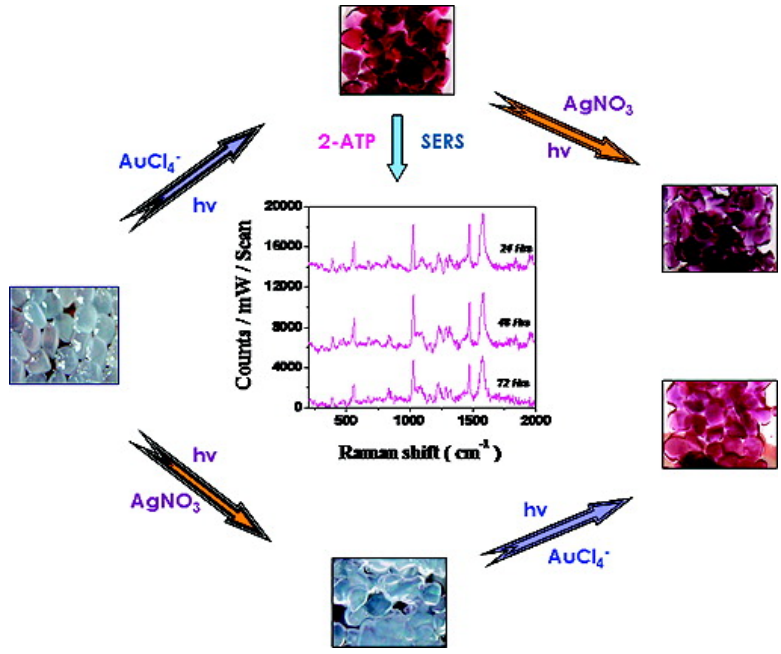

More About This Article

Additional resources and features associated with this article are available within the HTML version:

- Supporting Information
- Access to high resolution figures
- Links to articles and content related to this article
- Copyright permission to reproduce figures and/or text from this article

View the Full Text HTML

The Journal of Physical Chemistry C is published by the American Chemical Society. 1155 Sixteenth Street N.W., Washington, DC 20036

Alginate Gel-Mediated Photochemical Growth of Mono- and Bimetallic Gold and Silver Nanoclusters and Their Application to Surface-Enhanced Raman Scattering

Sandip Saha,[†,‡] Anjali Pal,[*,†] Surojit Pande,[‡] Sougata Sarkar,[‡] Sudipa Panigrahi,[‡,§] and Tarasankar Pal[‡]

Departments of Civil Engineering and Chemistry, Indian Institute of Technology, Kharagpur 721302, India

Received: December 19, 2008; Revised Manuscript Received: February 16, 2009

Polysaccharide alginate gel beads have been used as a template for photochemical growth of monometallic and bimetallic Au and Ag manoclusters. The gel served both as a reductant under photoirradiation and as a stabilizer. Fourier transform infrared (FTIR) analysis indicated that the secondary hydroxyl function reduced the Au(III) and Ag(I) to their metallic state with the concomitant oxidation of the hydroxyl function to carbonyl group. X-ray diffraction (XRD), scanning and transmission electron microscopy (SEM and TEM), energy-dispersive X-ray spectrometry (EDX) analyses were used to characterize nanoparticle structure, size, and morphology. The effectiveness of this alginate gel-stabilized nanoparticles as substrate toward surface-enhanced Raman scattering (SERS) detection was evaluated by use of two probes, 2-aminothiophenol and 1,10-phenanthroline. Intensity of SERS signals was a function of analyte adsorption as evidenced from UV−visible absorption spectroscopy. Among all the substrates, alginate-stabilized Au has been found to be the best for SERS detection. The enhancement factors are in the range of 10^4 and the detection limits are in the subpicogram level.

Introduction

Noble metal nanoparticles have drawn immense attraction due to their potential applications as catalyst,[1] electronic material,[2] DNA detector,[3] substrates for surface-enhanced Raman spectroscopy (SERS),[4] and in other domains of high technology and medicine. Unlike many other metals, nanosized Au and Ag can strongly interact with visible light and show unique behavior.[4d] They are extensively studied in the field of SERS. The light scattering property of these nanosized metal particles depends on the size, shape, and state of aggregation.[5a,b] In recent years, attention has been paid toward bimetallic nanoparticles for SERS detection. These bimetallic nanoparticles sometimes show unique behavior because of their modified electronic structure and optical properties.[5c] Depending on the distribution mode of two elements, different types of alloy such as random alloy, alloy with intermetallic compounds, cluster-in-cluster, and core−shell structures can be obtained. The presence of two metallic elements often causes an improvement in physical and chemical properties.[6]

Synthesis of metal nanoparticles in a confined environment, such as in a polymer network, either natural or synthetic, leads to precise control of the nanoparticle shape, size, three-dimensional architecture, etc.[7] Strategies to control the shape, size, and assembly of nanoclusters often employ template-driven synthesis. Numerous biological systems such as proteins,[8a] polysaccharides,[8b] DNA,[3,8c] or peptides[8d] have already been introduced to direct the growth of such nanoparticles. Among the large group of possible templates for nanoparticle growth, alginic acid exhibits several interesting features. This natural polysaccharide, which is a renewable biological resource available from brown marine algae (Phaeophyceae), is a very cheap and environmentally friendly material having immense use in food material and in pharmacy. Another important property is its gel-forming capability induced by bivalent metal ions such as Ca^{2+}, and this gel can be used as a biosorbent.[9a,b] Also, the presence of functionalities such as carboxylate and hydroxyl widens its applicability as a chemically active species. Moreover, the shape of the gel can be regulated, which may find application in liquid crystal display, microreactors, synthesis of materials with unique crystal structure,[9c] and tissue engineering.[9d] In addition to this, the entrapment of enzymes and/or cells in alginate is one of the simplest methods of immobilization.[10] These properties leave immense scope for alginate to be studied as a scaffold for metal nanoparticle formation, to be applied in medicine and drug delivery, and as a potential substrate for SERS analysis. Thus it may finally lead to a smart gel, a new generation biomaterial.

Alginic acid is a linear polysaccharide containing 1,4-linked β-D-mannuronic acid (M) and α-L-guluronic acid (G) in a nonregular order. Physical properties and its high affinity toward divalent atoms are mainly controlled by the macromolecular configuration, which depends on the ratio of M and G residues. An "egg box"-like gel network is formed in the presence of divalent cations such as Ca^{2+}. There are not many reports on alginate-stabilized nanoparticles, excepting a few. These include noble metal nanoparticles, such as Au[11a,b] and Au−Ag,[11c] prepared in aqueous sodium alginate, and nanoparticles such as Au and Ag[9b]and Co and Ni,[11d,e] synthesized in calcium alginate gel. Other than this, alginate has been used for magnetic iron oxide preparation also.[11f] Basically, two methods prevail. In the first method, metal is incorporated through gelation (that means the concerned metal ion is used instead of Ca^{2+} as gelation inducer). In the second method, after gelation is complete, the metal ions are incorporated in the gel through diffusion. In either case a reduction step is the next prerequisite. Very recently it has been shown that incorporation of already-

* To whom correspondence should be addressed: e-mail anjalipal@civil.iitkgp.ernet.in.
† Department of Civil Engineering.
‡ Department of Chemistry.
§ Present address: 4113 Centre for Biotechnology & Interdisciplinary Studies, Rensselaer Polytechnic Institute, Troy, NY 12180.

10.1021/jp811235m CCC: $40.75
Published on Web 04/14/2009

prepared gold nanorods[11g] into calcium alginate gel is also possible.[11h] The interest of using solid support or gel structure for nanoparticles formation is that it will stabilize the nanoparticles to a greater extent compared to sol and it will offer easy handling procedure. Polystyrene beads are known to serve as an excellent solid support for colloidal metal deposition.[12−14] The presence of two or more metals in close proximity may modify the optical, catalytic, and magnetic properties; for example, in core−shell structure, the shell may influence the properties of the nanomaterials in the core.[12]

Since the SERS discovery,[15a−d] SERS has been established to be a valuable analytical technique because of the very narrow, highly resolved bands associated with the Raman scattering. Interest is growing more and more to understand the mechanism behind SERS. Electromagnetic enhancement (EM) and chemical enhancement (CM) are the two crucial and fundamental mechanisms for SERS. Numbers of experiments were carried out in solution phase to understand the SERS effect. In most cases Au and Ag nanoparticles are used as the substrate. An electric field of surface plasmon is induced when light falls on the metal surface and the adsorbed molecule shows a transition moment under this electric field. This is known as EM mechanism.[15e] On the other hand, when a layer of molecules is adsorbed on the metal surface, a charge transfer interaction between the first layer of metal atoms and the adsorbed molecules is considered a chemical effect.[15f,g] Both mechanisms and even others can contribute simultaneously to the SERS enhancement to a certain extent, which is dependent on the experimental conditions, for example, the nature and morphology of the metallic nanoparticles and other factors. Till now, exhaustive efforts have been made toward the development of practical substrates to investigate the SERS effect. These include silver particles on quartz posts,[15h] metal island films,[15i] silver island films,[15j] metal-coated microsphere-based substrates,[15k] polymer-coated substrates,[15l] etc.

The present work addresses the synthesis of mono- and bimetallic Ag and Au nanoclusters on calcium alginate (CA) gel beads via a photoactivation technique and their applications to SERS. These are the first results in the line of research aimed at determining the SERS effect of such photochemically deposited mono- and bimetallic nanoclusters in alginate gel.

Experimental Section

Reagents. All the reagents were of AR grade. Sodium alginate was purchased from LOBA Chemicals. Silver nitrate and calcium chloride was obtained from SRL. $HAuCl_4$ was purchased from Aldrich. Milli Q water was used throughout the experiments. 2-Aminothiophenol (2-ATP) and 1,10-phenanthroline (1,10-phen) were purchased from Merck and were used without further purification.

Preparation of Calcium Alginate Gel Beads. A schematic of CA gel bead preparation is shown in Figure 1. In a typical procedure,[9a] freshly prepared aqueous sodium alginate solution (100 mL, 0.4 wt %) was added dropwise through a 50-ml Borosil buret to freshly prepared 0.1 M $CaCl_2$ solution (150 mL) under gentle stirring. The presence of Ca^{2+} initiates cross-linking instantly. Each droplet took the shape of a spherical bead. An aliquot of 1 mL of sodium alginate solution could produce ∼17 spherical CA beads under the experimental conditions. The beads were left in aqueous $CaCl_2$ solution for 1 h after the addition of sodium alginate solution was complete. Later, they were filtered and washed with plenty of Milli Q water. Again the beads were protonated in 30 mL of 0.1 M HNO_3 solution, washed thoroughly with water, and stored under

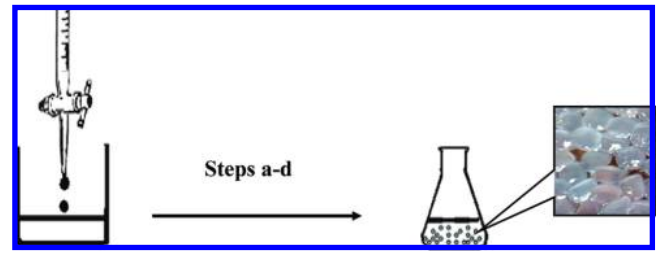

Figure 1. Schematic for preparation of CA beads: (step a) Addition of aqueous sodium alginate to aqueous $CaCl_2$ to form CA beads; (step b) protonation of the beads; (step c) further cross-linking in beads for more stabilization; (step d) beads stored in Milli Q water for further use. Each step was followed by thorough washing of the beads with Milli Q water.

100 mL of 0.1 M $CaCl_2$ solution for further cross-linking to achieve more stability. After 24 h of cross-linking, again they were washed with sufficient Milli Q water to make them chloride- and nitrate-free. Finally, they were stored under Milli Q water for further use. Calcium loading was estimated to be 14 mg/g in dry beads by inductively coupled plasma mass spectrometry (ICP-MS). The loss of weight after drying was ∼98% and it was accompanied by a diameter reduction of alginate bead from 3.5 to 2.0 mm.

Preparation of Monometallic Au on Calcium Alginate (Au-CA), Monometallic Ag on Calcium Alginate (Au-CA), Bimetallic Ag on Au-CA (Ag@Au-CA), and Bimetallic Au on Ag-CA (Au@Ag-CA), Beads. A simple photoactivation technique was followed for preparation of metal-coated CA beads. In all cases beads were taken as the core to stabilize the surface of nanoparticles evolved. For Au-CA bead preparations, approximately 500 beads were incubated, at room temperature in 1.2 mL solution of 1.0 mM $AuCl_4^-$ for 3 h. After incubation, the beads were irradiated with UV light for 40 min, with gaps of 10 min between each 10 min of irradiation. Similar steps were taken for preparing Ag-CA beads with $AgNO_3$ solution (1.0 mM). Following the same procedure, beads were coated in a stepwise fashion but successively three times, with fresh $HAuCl_4$ and $AgNO_3$ solution for Au and Ag coating, respectively.

For bimetallic deposition, Au-CA and Ag-CA beads were used for further coating with Ag and Au nanoparticles, respectively. The coating by the second metal was also repeated for three times again in a stepwise manner. After the completion of coating by one metal, the beads were thoroughly washed with Milli Q water and used for the next coating.

SERS Analysis with Au-CA, Ag-CA, Au@Ag-CA, and Ag@Au-CA Beads as Substrates and 2-Aminothiophenol and 1,10-Phenanthroline as Probes. For SERS studies, metal-loaded CA beads were kept for incubation separately in ethanolic solution of 2-ATP or 1,10-phen (in the concentration range of $10^{-3}−10^{-5}$ M) and SERS spectra were accumulated after 24, 48, and 72 h of incubation. Spectra were recorded after beads were transferred over a glass slide followed by 30 min of air drying.

Instruments. Absorption spectra were recorded on a Spectrascan UV 2600 spectrophotometer (Chemito) equipped with a 1-cm well-stopped quartz cuvette. Fourier transform infrared (FTIR) spectra were collected in transmittance mode on a Perkin-Elmer Spectrum l RX1 FTIR instrument. Solid CA beads were ground with KBr, and IR spectra were recorded. The ICP mass instrument (Optima 2100DV spectrometer, Perkin-Elmer) was used to estimate calcium loading on dry beads. A scanning electron microscope (SEM) Quanta 200 (FEI Co.) instrument was used for SEM analysis. High-resolution transmission

electron microscopic (HRTEM) images and energy-dispersive X-ray were recorded on a ZEOL ZEM 2010 with an accelerating voltage of 200 kV. The Oxford Instruments energy-dispersive X-ray (EDX) INCA energy system was connected with transmission electron microscopy (TEM). Raman spectra were collected by use of a Reinshaw Raman confocal system spectrophotometer equipped with an integral microscope. He−Ne (663 nm) laser excitation source with a Peltier-cooled (−70 °C) charge-coupled device (CCD) camera was used. Laser power for sample analysis was 1 mW, and spectra were collected at 20 s accumulation for a single time at 663-nm excitation. Data for X-ray diffraction (XRD) analysis were collected from an XD-D1 Shimadzu X-ray diffractometer with an X-ray source Cu (Kα = 1.540 56). Photoirradiation was carried out with a UV light (15 W; Philips) irradiating at ∼365 nm wavelength.

Results and Discussion

Photochemical Formation of Metal Nanoparticles on CA Beads. Natural carbohydrate-based biopolymers, which are nontoxic in nature, are being used for nanoparticle stabilization for their potential applications in biomedical fields.[16,17] Although both chemical and photochemical routes are available for reduction purposes, chemical processes are more common. However, the use of toxic chemicals such as hydrazine, sodium borohydride, etc., as chemical reductants poses potential environmental and biological risks. Synthetic procedures adopted for metal nanoparticle (mono- and bimetallic) preparations by photoirradiation in carbohydrate-based polymers follow a very simple technique and recently have been well documented.[18,19] The abundant hydroxyl groups present in carbohydrates can bring about reduction efficiently and at the same time can stabilize the particles within the matrix. The alginate gel-based photochemical synthesis of nanoparticles has been adopted in the present work as a "green approach". Earlier studies[9b] showed that adsorption of gold and silver ion on alginate gel and further keeping for long times can lead to Au and Ag nanoparticle formation, although aggregation was noticed in this case.

The carboxylic acid dissociation constants (pK_a) of M and G in alginic acid are 3.38 and 3.56, respectively.[9b] When the pH exceeds the pK_a, carboxylic groups progressively remain less protonated or completely deprotonated depending on the prevailing pH. The carbohydrate units M and G play a key role in photochemical reduction of metal ions, and the alginate gel acts as a stabilizer. The nanoparticles remain stable in alginate for months together under ambient conditions. Only a UV source of certain wavelength can invoke the formation of nanoparticles in alginate.

Time-dependent studies on the adsorption of $HAuCl_4$ on CA beads in the dark and further photoreaction under UV light were performed, and the UV−visible spectral behavior in the solution phase with time was monitored. Curve a in Figure 2 shows the absorption spectrum of $HAuCl_4$ in the absence of CA beads. The characteristic peaks appearing at 220 and 290 nm are due to metal-to-ligand charge transfer (MLCT) in $AuCl_4^-$.[20] Upon addition of CA beads and standing for 3 h under dark conditions, these two peaks disappeared completely (curve b in Figure 2) showing absorption at a lower-wavelength region, and the yellow color of $HAuCl_4$ also vanished. This indicates slow adsorption of $HAuCl_4$ onto CA beads. The beads were then photoirradiated with UV light up to 30 min. Absorption spectra of the solution after 10, 20, and 30 min of irradiation are shown as curves c−e in Figure 2. Spectra show that upon 10 min of irradiation there is still a decrease in absorption in the range <220 nm compared to absorption before irradiation. With

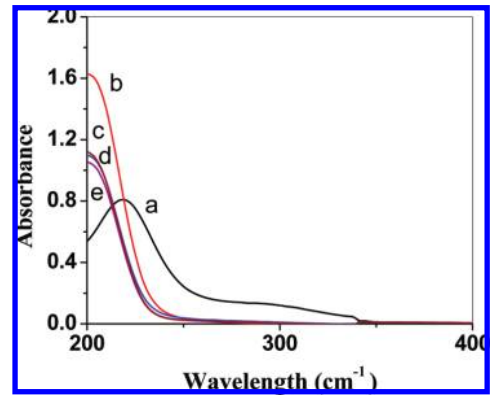

Figure 2. UV−vis spectra of (a) $HAuCl_4$ alone, before adsorption; (b) $HAuCl_4$ after 3 h of adsorption on CA beads in the dark; and (c−e) $HAuCl_4$ after 3 h of adsorption followed by 10, 20, and 30 min of UV irradiation, respectively.

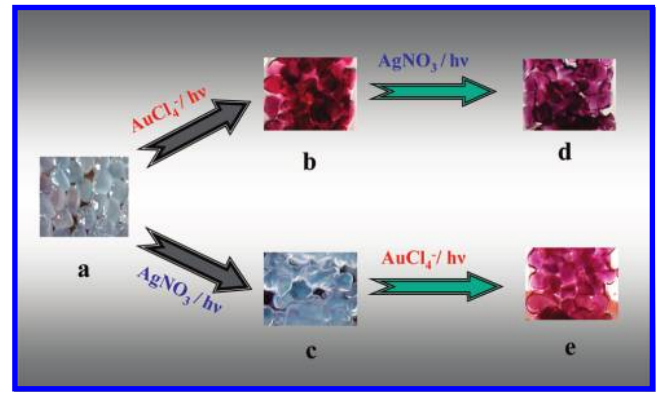

Figure 3. Photograph of various CA-stabilized metal nanoparticles: (a) CA, (b) Au-CA, (c) Ag-CA, (d) Ag@Au-CA, and (e) Au@Ag-CA beads.

further irradiation up to 40 min, however, there was no change. This indicates that probably 10 min irradiation was sufficient to get deposition of Au(0) onto the CA bead, but to ensure complete deposition, a procedure with 40 min of irradiation was undertaken in our experiments. To prepare Ag-CA beads, a similar procedure was adopted and in that case $AgNO_3$ solution was used. The CA beads after deposition of one metal were subjected to deposition of the other metal to prepare Ag@Au-CA beads and Au@Ag-CA beads. The deposition of Au nanoparticles during photoirradiation was also clearly visualized as the beads turned to red. The deposition was done three times to make beads more effective for SERS analysis. In the case of Ag-CA beads no color change has been noticed, and for bimetallic CA beads a nice bluish-pink color was obtained after photoirradiation (Figure 3).

Surface plasma resonance (SPR) data would be important for understanding the different SERS behaviors of the nanoparticles. UV−visible absorption spectrum of Au-CA, Ag-CA, Au@Ag-CA, and Ag@Au-CA were recorded in gel phase and are shown in Figure 4 as curves a−d, respectively. Au-CA and Ag-CA show their usual characteristic SPR bands at 532 and 405 nm, respectively. The appearance of a single band for Au@Ag-CA at λ_{max} = 540 nm (which is slightly red-shifted compared to that of Au-CA) indicates that the particles are larger compared to those present in Au-CA and that Au is in the shell. The spectrum of Ag@Au-CA shows, along with its usual band at 412 nm for Ag(0), a shoulder at ∼512 nm. This indicates that Ag is present as shell and Au is in the core. The red shift of the band here due to Ag(0) compared to that of Ag(0) present in

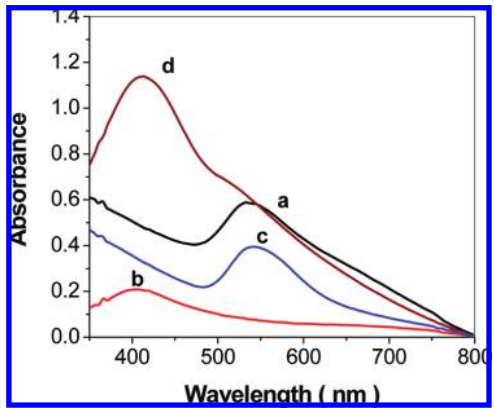

Figure 4. UV−vis spectra of (a) Au-CA, (b) Ag-CA, (c) Au@Ag-CA, and (d) Ag@Au-CA beads.

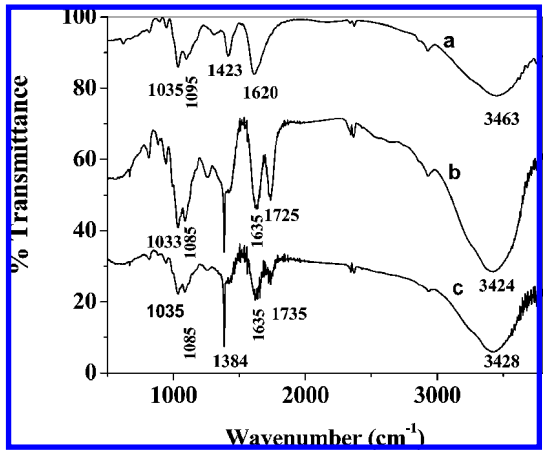

Figure 5. FTIR spectra of (a) CA, (b) Au-CA, and (c) Ag-CA beads.

Ag-CA reveals a larger size. All spectra are in conformity with the colors of the beads. The spectral nature has a close resemblance to those obtained for mono- and bimetallic Au−Ag nanoparticle dispersions in β-cyclodextrin as reported earlier.[6]

Fourier Transform Infrared Studies. Participation of alginate as a reductant under photoirradiation can be explained by comparing the FTIR spectra of CA before (curve a in Figure 5) and after (curves b and c in Figure 5) photoreaction with $HAuCl_4$ and $AgNO_3$. Curve a shows bands at 1620 and 1423 cm^{-1}, which are characteristic for stretching vibrations of carboxylate anion present in CA.[9b] Strain vibration of >C═O should occur at ∼1705 cm^{-1}. It has appeared in these gels at wavelengths lower than 1650 cm^{-1}, indicating the presence of intramolecular hydrogen bridges.[9b] Formation of carbonyl functionality after photoreduction of $HAuCl_4$ and $AgNO_3$ can be clearly visualized by the appearance of a new band at 1725 cm^{-1} in the FTIR spectrum of Au-CA (curve b, Figure 5), and at 1735 cm^{-1} in Ag-CA (curve c, Figure 5). This indicates the presence of a six-membered cyclic ketone in both cases. Here a process is taking over where secondary -OH groups present in the M and/or G skeleton undergo oxidation to >C═O and metal ions undergo reduction to form metal nanoparticles. Bands in the range 3424−3463 cm^{-1} for CA beads and metal-coated CA beads indicate the presence of -OH groups in all cases. The reduction of Au(III) to Au(0) caused by secondary -OH functionality and its concomitant oxidation to carbonyl group is not abnormal and could early be seen in case of sugar-persubstituted poly(amidoamine) dendrimers.[21] The reducing property of catechol moiety in dopamine hydrochloride[22] and the primary hydroxyl group present in Triton X-100[23] have also been exploited for preparation of gold nanoparticles via photoactivation. Here the catechol is oxidized to quinone and the primary hydroxyl group in Triton X-100 was oxidized to a carboxylic acid function.

X-ray Diffraction Studies for Particle Characterization. The crystallinity of nanoparticles deposited on the surface of CA was investigated for Au-CA, Ag-CA, Ag@Au-CA, and Au@Ag-CA by X-ray diffraction (XRD) studies. XRD data confirmed the crystalline nature of the CA-stabilized metal nanoparticles. The CA bead-stabilized metal nanoparticles were dried under vacuum and used for X-ray analysis. A typical XRD pattern of as-prepared Au-CA beads (Figure 6A) shows broad Bragg's reflections at $2\theta = 38.2°$, 44.3°, 64.5°, 77.4°, and 81.5°, corresponding to {111}, {200}, {220}, {311}, and {222} lattice planes, respectively, for the face-centered cubic (fcc) structure of immobilized gold nanoparticles. It is worth mentioning that mono- and bimetallic nanocomposites of Au and Ag have similar XRD patterns owing to the comparable lattice constants (0.408 vs 0.409 nm). Thus the XRD patterns could not provide definitive evidence for the formation of bimetallic nanostructure. However, the XRD pattern of the bimetallic particles is consistent with the XRD patterns of monometallic components. No diffraction peaks corresponding to silver oxide are observed. Furthermore, the entire XRD pattern shows that the particle size is in the nanometer range without any aggregation.[24] Figure 6B−D shows the XRD patterns of Ag-CA, Au@Ag-CA, and Ag@Au-CA beads. In all cases the peaks appeared in the same region, indicating that all these crystals are fcc type.[25]

Scanning and Transmission Electron Microscopic Studies. Scanning electron microscopy (SEM) study was done on CA beads (Figure 7A), and metal-coated CA beads (Figure 7B−E), showing different morphologies of the particles. A brighter surface was observed for the bimetallic CA beads that have outermost Ag coating.

Particle sizes and shapes of monometallic and bimetallic nanoparticles were determined from the TEM images (Figure 8). The particles were spherical and the size ranged within 8 ± 2 nm and 12 ± 4 nm for Au and Ag particles, respectively. In the case of Au@Ag-CA nanoparticles the size varied in the range of 21−28 nm, and for Ag@ Au-CA it was 23−32 nm. In this context it is worth mentioning that a similar spherical nature was also observed for Au and $Au_{core}-Ag_{shell}$ nanoparticles synthesized in sol phase with sodium alginate via a photochemical approach.[11a,c] EDX studies on the bimetallic particles show that the Au:Ag (atomic) ratio is 1:0.25 for Au@Ag-CA and 1:9 for Ag@Au-CA. This also confirms the evolution of bimetallic particles in the CA gel bead by the present method.

SERS Studies on Mono- and Bimetallic CA Beads. The SERS activity of metal colloids depends on their size, shape, and the nature of aggregation. The aggregation is important to produce "hot junctions", which can function as an electromagnetic "hot spot" analogous to those predicted to exist in large fractal aggregates.[26,27] The "hot spot" generation can be induced either by adding extra electrolyte to the medium[28] or by the probe itself.[6] However, this may have a destabilizing effect on the sol. Destabilization can also occur when the sol is kept for longer times, due to the formation of bigger particles. This often causes practical problems with SERS detection in terms of reproducibility. SERS studies on solid bead-stabilized nanoparticles are less explored. In our present study 2-ATP and 1,10-phen was chosen as probe molecules to evaluate the efficacy of alginate gel-stabilized mono- and bimetallic Au−Ag particles, and no extra electrolyte was introduced. SERS of 1,10-phen

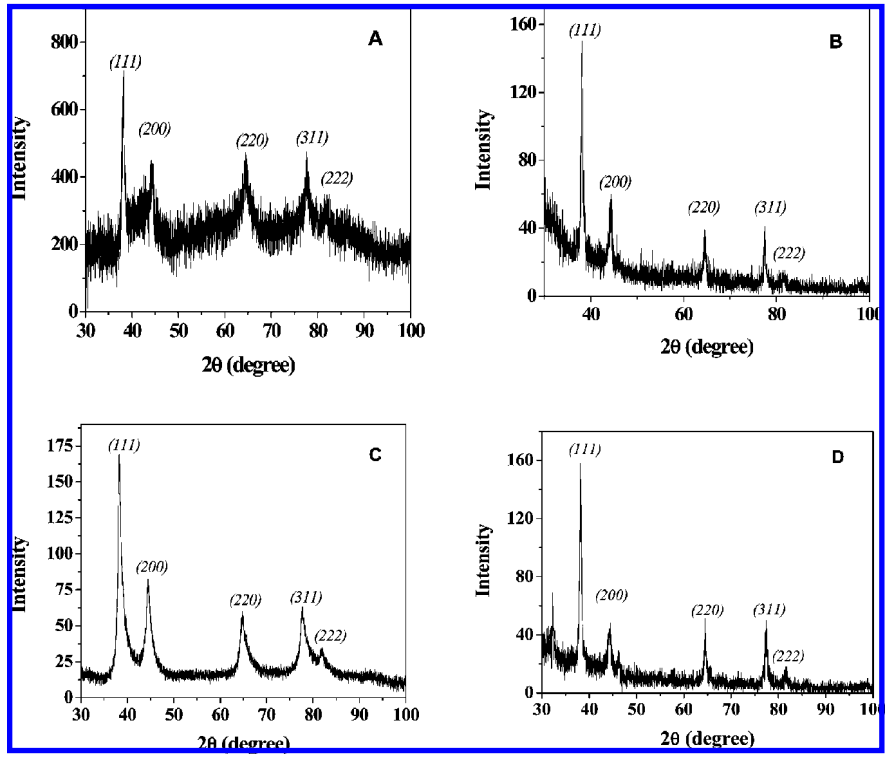

Figure 6. XRD of (A) Au-CA, (B) Ag-CA, (C) Au@Ag-CA, and (D) Ag@Au-CA beads.

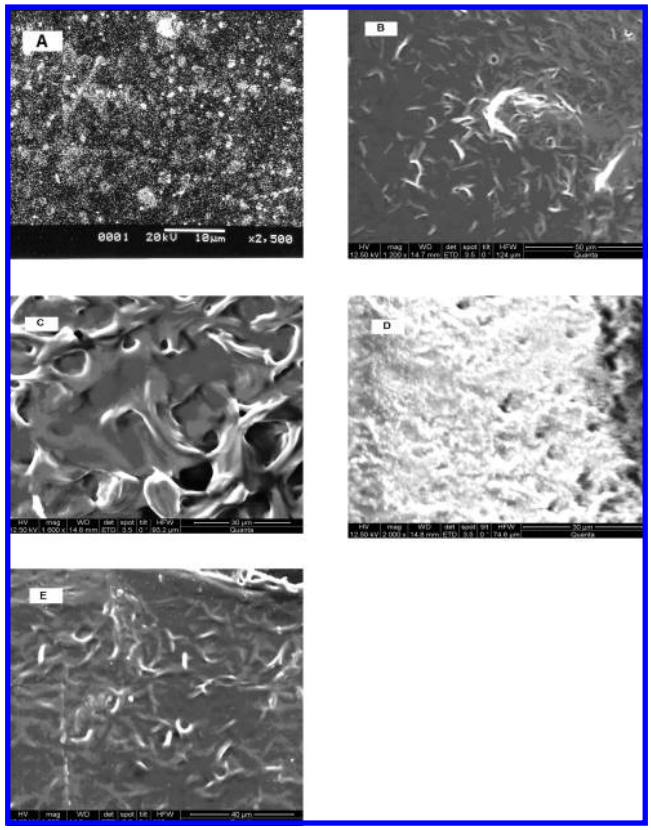

Figure 7. SEM images of (A) CA, (B) Au-CA, (C) Ag-CA, (D) Ag@Au-CA, and (E) Au@Ag-CA beads.

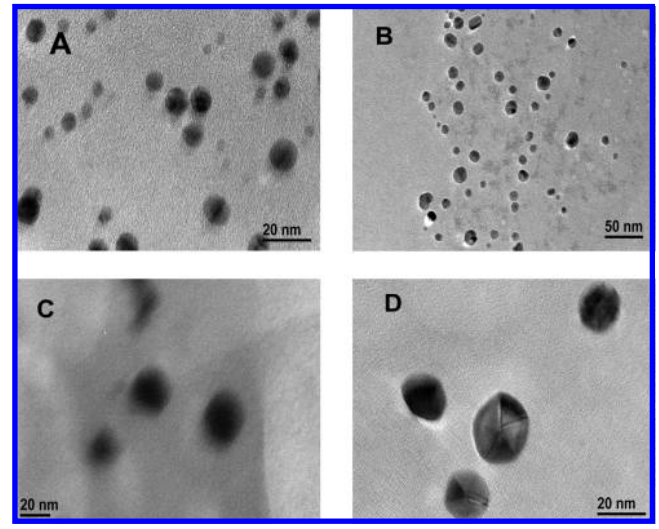

Figure 8. TEM of (A) Au-CA, (B) Ag-CA, (C) Ag@Au-CA, and (D) Au@Ag-CA beads.

was studied previously on silver sol[29] and on gold electrode surface[30] and in core−shell architecture of gold−silver in β-cyclodextrin.[6] On the other hand, SERS of 2-ATP was studied on aggregated silver nanoplates[31] and on aggregated gold nanorods.[32a] This is the first time calcium alginate-stabilized Au, Ag nanoparticles have been studied as a substrate for SERS. SERS spectra of 1,10-phen and 2-ATP on Au-CA beads are shown in Figure 9, and Raman peaks for both molecules are assigned and compiled in Tables 1 and 2. Since SERS band intensities are dependent on adsorption of probe molecules on the substrates, the time-dependent adsorption behavior of 2-ATP and 1,10-phen was monitored by solution-phase absorption spectroscopy (Figure 10). Figure 10A shows that in solution the intensity of the band at $\lambda_{max} = 338$ nm for 2-ATP decreases at 24 h compared to that at 0 h, indicating that adsorption of 2-ATP takes place on Au-CA beads. The adsorption increases with time up to 72 h of incubation. The best SERS, however, is observed at 48 h (as shown in Figure S1 in Supporting Information). This might be due to degradation of 2-ATP on the metal substrate. On the other hand, for 1,10-phen, as observed in the time-dependent absorption spectrum (Figure 10B), the adsorption is best at 48 h (≈72 h) as compared to

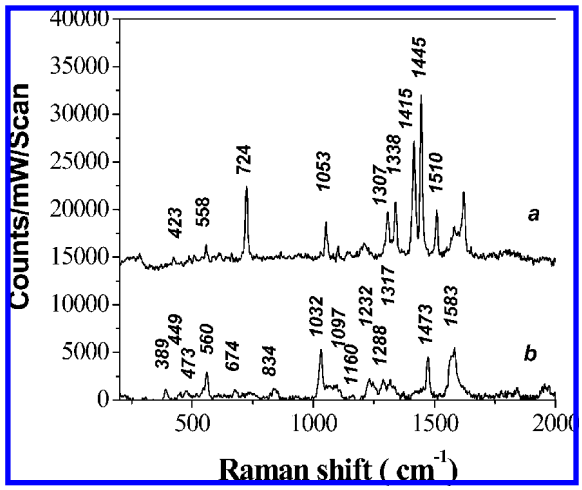

Figure 9. SERS spectra of ethanolic solutions (1.0 mM) of (a) 1,10-phen and (b) 2-ATP on Au-CA beads.

TABLE 1: Assignments of Major SERS Peaks of 1.0 mM 1,10-Phen on Nanoparticle-Coated CA Beads

	SERS peak (cm^{-1})			
vibration	reference[a]	Au-CA	Ag@Au-CA	Au@Ag-CA
ν_2 (A_1)	420	423	421	418
ν_3 (A_1)	555	558	556	557
ν_4 (A_1)	721	724	720	720
ν_6 (A_1)	1051	1053	1049	1048
ν_{12}(A_1)	1300	1307	1301	1300
ν_{13}(A_1)	1342	1338	1343	1344
ν_{14}(A_1)	1407	1415	1409	1409
ν_{15}(A_1)	1448	1445	1448	1445
ν_{16}(A_1)	1512	1510	1513	1512

[a] Reference values are taken from ref 32b.

TABLE 2: Assignments of Major SERS Peaks of 1.0 mM 2-ATP on Nanoparticle-Coated CA Beads

	SERS peak (cm^{-1})			
vibration	reference[a]	Au-CA	Ag@Au-CA	Au@Ag-CA
γ(C−N)			240	
δ(C−S)	386	389	398	390
γ(C−C)	444	449	447	452
ν(C−C)	472	473	473	470
δ(C−C)	556	558	560	559
δ(C−C)	672	674	678	679
ring breathing	834	834	820	825
δ(C−H)	1027	1032	1033	1035
δ(C−C)	1050	1053	1055	1054
$\delta(NH_2)$	1078	1097	1095	1081
δ(C−H)	1160	1160	1163	1131
δ(C−H)	1226	1232	1229	1233
ν(C−N)	1282	1288	1288	1292
ν(C−N)	1309	1317	1327	1326
ν(C−C)	1471	1473	1473	1473
ν(C−C)	1562	1583	1583	1582

[a] Reference values are taken from ref 32a.

that at 24 h, and this has been significantly observed in the SERS enhancement at 48 h over 24 h (as presented in Figure S2 in Supporting Information). In this case also the peak weakens when kept further for another 24 h. This indicates that the 1,10-phen probe molecule is either decomposed[32b] on the surface or the surface is deactivated over time. From these results it can be assumed that SERS signals are a function of analyte adsorption onto the substrate. SERS spectra for both probe molecules could be obtained in the range $10^{-3}-10^{-5}$ M.

In general, it is known that Ag monometallic nanoclusters are good SERS-active substrates, whereas gold monometallic nanoclusters are generally less active. However, the electronic ligand effect can influence the SERS activity of one metal in bimetallic nanoparticles.[33,6] In order to study the SERS effect due to deposition of one metal over the other (i.e., in a bimetallic substrate), the as-prepared Ag@Au-CA and Au@Ag-CA beads were tested with both probes, and it is seen that both molecules are active for SERS on both types of bimetallic particles. At this point it should be emphasized that in our case monometallic Ag-CA substrate does not work. The particles were not aggregated (as is clear from TEM) and the probe molecule does not induce aggregation (which is a prerequisite to observe SERS).[29,31] This relates to the fact that the particles are embedded in gel structure. As observed from Figure 4, the nonaggregated Ag particles do not have plasmon absorption in resonance with the excitation light source. Another simple reason may be that Ag particles are more protected by alginate, thus hindering analyte adsorption. As opposed to Ag-CA, other alginate-stabilized nanostructures have absorption bands in resonance with the laser source, thus showing good SERS activity. In our earlier studies[6] on β-cyclodextrin-based Au and Ag mono- and bimetallic nanostructures in solution phase, we showed that SERS activity is in the order $Au_{core}-Ag_{shell}$ > Ag > $Ag_{core}-Au_{shell}$ > Au. In the present study, however, it is noticed that with both probe molecules Au-coated bead stands best and overpowers the other nanostructures. Also it is important to mention that beads older than 2 months show less efficiency toward SERS. Alginates are biodegradable polymers so these results may not be surprising.

It is important to notice that, for bimetallic-CA substrates (Au@Ag-CA and Ag@Au-CA) with ethanolic 1.0 mM 2-ATP, the same characteristic bands were obtained (Table 2). Time-dependent SERS of 2-ATP with Ag@Au-CA beads as substrate (as observed in Figure S3 in Supporting Information) showed that the bands are comparatively weak at 24 h and become optimal at 48 h. Decrease in peak intensity, however, upon further keeping up to 72 h may be due to decomposition of the 2-ATP molecule on the outermost silver surface.

To evaluate the performance of the Au@Ag-CA bead as the SERS substrate, time dependent studies were carried out using 1,10-phen molecule. In this case also 48 h of incubation gives the best enhancement (as shown in Figure S4 in Supporting Information).

All these studies indicate that both probe molecules are active toward all substrates except Ag-CA, and maximum enhancement is observed at 48 h of incubation. In this context it is worth mentioning that CA beads alone did not show any Raman band in the experimental concentration range (10^{-3} M) of the probe molecules. SERS intensities at selected peaks of both probes, obtained at various time intervals with various substrates used in our study, are depicted in Figure 11.

Effect of pH on SERS. For SERS effects to occur, adsorption of probe molecules on the surface of metal nanoparticles is necessary, and the development of surface charge on nanoparticles determines the feasibility of adsorption of analyte molecule.[34] Similar charges on both adsorbate and adsorbent make the adsorption unfavorable. In systems where nanoparticles are strongly stabilized by solid or polymeric compounds, the nature of adsorption may be somewhat different from that of a colloidal solution. An important factor affecting SERS is the pH of the medium.[35] With a view to evaluating the effect of pH on SERS for the alginate-supported nanoparticles, Au-CA beads were examined under different pH conditions (in the range 2−11)

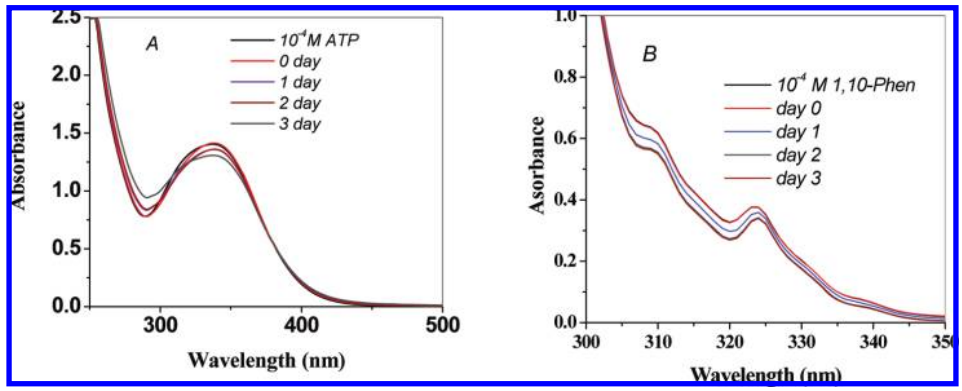

Figure 10. Time-dependent UV−vis absorption spectroscopic studies on the adsorption of ethanolic (0.1 mM) solution of (A) 2-ATP and (B) 1,10-phen on Au-CA beads.

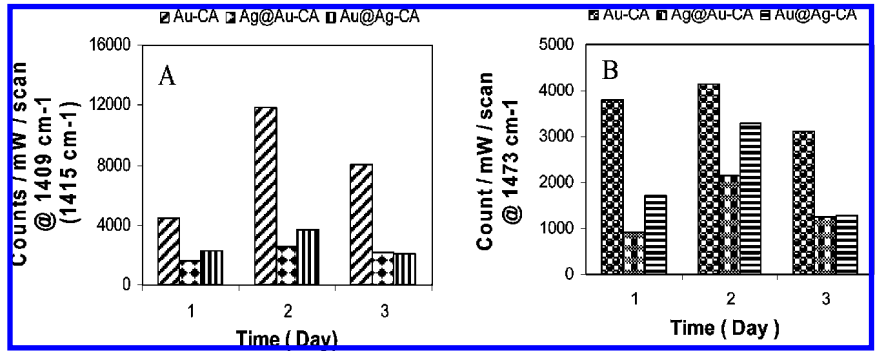

Figure 11. Comparative study on SERS of 1.0 mM ethanol solutions of (A) 1, 10-phen and (B) 2-ATP with Au-CA, Ag@Au-CA, and Au@Ag-CA beads as substrates.

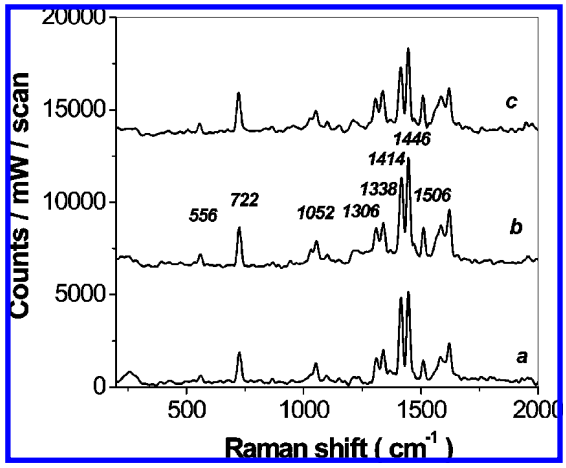

Figure 12. Effects of pH on SERS of 1,10-phen on Au-CA beads at (a) pH = 2, (b) pH = 8, and (c) pH = 11.

with the probe 1,10-phen. In this wide range of pH the spectral nature and peak positions of 1,10-phen remain unchanged. This indicates that the mode of adsorption does not change with pH. But increasing pH has a negative effect on SERS intensity (Figure 12). The decrease of intensity, however, is more prominent at pH 11. The reason may be that at higher pH the -COOH groups in the alginate are ionized to a greater extent. Because adsorption of 1,10-phen is supposed to be via the nitrogen donor points,[30] thus interaction between the donor nitrogen of 1,10-phen and the substrate becomes unfavorable, resulting in a weaker SERS effect at higher pH.

Estimations of Enhancement Factor and Detection Limit. Calculation of analytical enhancement factor (AEF)[36a] for both probe molecules with Au-CA substrate was done by comparing SERS intensity with nonenhanced Raman intensity (keeping other experimental conditions the same) and following the equation[31,36a,b]

$$\mathrm{AEF} = (I_{\mathrm{SERS}} C_{\mathrm{RS}})/(I_{\mathrm{RS}} C_{\mathrm{SERS}})$$

where I_{SERS} and I_{RS} were the respective SERS intensity (on Au-CA substrate) and normal Raman intensity, respectively for the analyte concerned. We have used the analyte concentration C_{RS}, which produces Raman signal I_{RS} under non-SERS condition as 0.1 M for both probe molecules. The analyte concentration for SERS intensity was 10^{-5} M for both 2-ATP and 1,10-phen. The 1032 cm^{-1} peak for 2-ATP in the SERS spectrum was selected for calculating the AEF of 2-ATP, and for 1,10-phen, the 724 cm^{-1} peak was selected. The AEF found was 6.6×10^4 for 2-ATP and 5.4×10^4 for 1,10-phen (a detailed discussion is given in Figure S5 in Supporting Information).

To estimate the detection limit of probe molecules on the newly developed substrate, it was necessary to know the extent of adsorption. This was found out with the help of UV−vis spectroscopy by using the standard calibration curve for the probes developed at their respective λ_{max}. Once the concentration of probe remaining in solution after adsorption is known, it is possible to find out the amount of probe adsorbed in the gel beads. If homogeneous distribution of the probe among the beads is assumed, the amount of probe per bead can be estimated. In our SERS study, one bead was placed on the glass surface and dried under ambient conditions. The area of the dried bead on the glass substrate was determined, and it was assumed that the whole amount of the probe is homogeneously distributed in this area. The laser illuminated only $1/10^6$ part of the bead. The detection limits of 2-ATP and 1,10-phen were subpicogram level.

Conclusions

Calcium alginate polymer gel beads were used for metal nanoparticle deposition, and finally their possible application as SERS substrate was evaluated. A UV photoactivation technique was used to develop the polymer-supported monometallic Au and Ag and bimetallic Au@Ag and Ag@Au substrates. The secondary hydroxyl group present in the alginate moiety took part in reducing Au and Ag photochemically, and in return it was oxidized to a carbonyl function as evidenced from FTIR analysis. The surface morphology was characterized by SEM studies. TEM analysis showed that the particles are spherical. From XRD analysis, the particle nature was found to be crystalline. The as-prepared metal-coated beads were examined as SERS substrates by use of the probes 2-ATP and 1,10-phen. Detailed comparative analysis revealed that the efficiency is in the order Au > Au@Ag > Ag@ Au. The Ag substrate failed to show any SERS activity. The effect of incubation time period on SERS up to 72 h showed that in all cases 48 h is the optimum time to get the best SERS effect. The enhancement factor was on the order of 10^4, and the detection limit was subpicogram level. The gel-stabilized particles are very stable.

Acknowledgment. We are thankful to UGC, New Delhi, India, and Indian Institute of Technology, Kharagpur, India, for financial assistance.

Supporting Information Available: Five figures showing time-dependent SERS of 2-ATP on Au-CA, 1,10-phen on Au-CA, 2-ATP on Ag@Au-CA, and 1,10-phen on Au@Ag-CA and discussion on AEF calculation. This material is available free of charge via the Internet at http://pubs.acs.org.

References and Notes

(1) (a) Pradhan, N.; Pal, A.; Pal, T. *Langmuir* **2001**, *17*, 1800–1802. (b) Mei, Y.; Lu, Y.; Polzer, F.; Ballauff, M. *Chem. Mater.* **2007**, *19*, 1062–1269. (c) Hayakawa, K.; Yoshimura, Y.; Esumi, K. *Langmuir* **2003**, *19*, 5517–5521.

(2) Li, Y.; Wu, Y.; Ong, B. S. *J. Am. Chem. Soc.* **2005**, *127*, 3266–3267.

(3) Nam, J.-M.; Thaxton, C. S.; Mirkin, C. A. *Science* **2002**, *295*, 1503–1506.

(4) (a) Li, X.; Xu, W.; Zhang, J.; Jia, H.; Yang, B.; Zhao, B.; Li, B.; Ozaki, Y. *Langmuir* **2004**, *20*, 1298–1304. (b) Sun, L.; Song, Y.; Wang, L.; Guo, C.; Sun, Y.; Liu, Z.; Li, Z. *J. Phys. Chem. C* **2008**, *112*, 1415–1422. (c) Pal, A.; Isola, N. R.; Alarie, J. P.; Stokes, D. L.; Vo-Dinh, T. *Faraday Discuss.* **2006**, *132*, 293–301. (d) Kamat, P. V. *J. Phys. Chem. B.* **2002**, *106*, 7729–7744.

(5) (a) El-Sayed, M. *Acc. Chem. Res.* **2001**, *34*, 257–264. (b) Kely, K. L.; Coronado, E.; Zhao, L. L.; Schatz, G. C. *J. Phys. Chem. B.* **2003**, *107*, 668–677. (c) Cui, Y.; Ren, B.; Yao, J.-L.; Gu, R.-A.; Tian, Z.-Q. *J. Phys. Chem. B.* **2006**, *110*, 4002–4006.

(6) Pande, S.; Ghosh, S. K.; Praharaj, S.; Panigrahi, S.; Basu, S.; Jana, S.; Pal, A.; Tsukuda, T.; Pal, T. *J. Phys. Chem. C.* **2007**, *111*, 10806–10813.

(7) Zhang, J.; Xu, S.; Kumacheva, E. *J. Am. Chem. Soc.* **2004**, *126*, 7908–7914.

(8) (a) Douglas, D.; Stark, V. T. *Inorg. Chem.* **2000**, *39*, 1828–1830. (b) He, J.; Kunitake, T.; Nakao, A. *Chem. Mater.* **2003**, *15*, 4401–4406. (c) Warner, M. G.; Hutchinson, J. E. *Nat. Mater.* **2003**, *2*, 272–277. (d) Reiss, B. D.; Mao, C.; Solis, D. J.; Tyan, K. S.; Thomson, T.; Belcher, A. M. *Nano Lett.* **2004**, *4*, 1127–1132.

(9) (a) Ibáñez, J. P.; Umetsu, Y. *Hydrometallurgy* **2002**, *64*, 89–99. (b) Torres, E.; Mata, Y. N.; Blazquez, M. L.; Munoz, J. A.; Gonzalez, F.; Ballester, A. *Langmuir* **2005**, *21*, 7951–7958. (c) Zheng, B.; Tice, J. D.; Ismagilov, R. F. *Anal. Chem.* **2004**, *76*, 4977–4982. (d) Sakai, S.; Masuhara, H.; Yamada, Y.; Ono, T.; Iijima, H.; Kawakami, K. *J. Biosci. Bioeng.* **2005**, *100*, 127–129.

(10) (a) Spettoli, P.; Bottacin, A.; Nuti, M. P.; Zamorani, A. *Am. J. Enol. Vitic.* **1982**, *33*, 1–5. (b) Coradin, T.; Livage, J. *C. R. Chim.* **2003**, *6*, 147–152.

(11) (a) Pal, A.; Esumi, K.; Pal, T. *J. Colloid Interface Sci.* **2005**, *288*, 396–401. (b) Gao, S.; Zhang, S.; Jiang, K.; Yang, S.; Lu, W. *Curr. Nanosci.* **2008**, *4*, 145–150. (c) Pal, A.; Esumi, K. *J. Nanosci. Nanotechnol.* **2007**, *7*, 2110–2115. (d) Brayner, R.; Vaulay, M. J.; Fievet, F.; Coradin, T. *Chem. Mater.* **2007**, *19*, 1190–1198. (e) Brayner, R.; Coradin, T.; Fievet-Vincent, F.; Livage, J.; Fievet, F. *New J. Chem.* **2005**, *29*, 681–685. (f) Gao, S.; Shi, Y.; Zhang, S.; Jiang, K.; Yang, S.; Li, Z.; Takayama-Muromachi, E. *J. Phys. Chem. C* **2008**, *12*, 10398–10401. (g) Sau, T. K.; Murphy, C. J. *Langmuir* **2004**, *20*, 6414–6420. (h) Mitamura, K.; Imae, T.; Saito, N.; Takai, O. *J. Phys. Chem. C* **2008**, *112*, 416–422.

(12) Pol, V. G.; Grisaru, H. *Langmuir* **2005**, *21*, 3635–3640.

(13) Dokoutchaev, A.; James, J. T.; Koene, S. C.; Pathak, S.; Surya Prakash, G. K.; Thompson, M. E. *Chem. Mater.* **1999**, *11*, 2389–2399.

(14) (a) Praharaj, S.; Nath, S.; Panigrahi, S.; Ghosh, S. K.; Basu, S.; Pande, S.; Jana, S.; Pal, T. *Inorg. Chem.* **2006**, *45*, 1439–1441. (b) Nath, S.; Ghosh, S. K.; Kundu, S.; Praharaj, S.; Panigrahi, S.; Basu, S.; Pal, T. *Mater. Lett.* **2005**, *59*, 3986–3989.

(15) (a) Fleischmann, M.; Hendra, P. J.; McQuillan, A. J. *Chem. Phys. Lett.* **1974**, *26*, 163–166. (b) Creighton, J. A.; Blatchford, C. G.; Albrecht, M. G. *J. Chem. Soc., Faraday Trans. 2.* **1979**, *75*, 790–798. (c) Jeanmaire, D. L.; Van Duyne, R. P. *J. Electroanal. Chem.* **1977**, *84*, 1–20. (d) Moskovits, M. *Rev. Mod. Phys.* **1985**, *57*, 783–826. (e) Kahl, M.; Voges, E. *Phys. Rev. B* **2000**, *61*, 14078–14088. (f) Ueba, H. *Surf. Sci.* **1983**, *131*, 347–366. (g) Otto, A.; Billmann, J.; Eickmans, J.; Ertürk, U.; Pettenkofer, C. *Surf. Sci.* **1984**, *138*, 319–338. (h) Vo-Dinh, T.; Meier, M.; Wokaun, A. *Anal. Chim. Acta* **1986**, *181*, 139–148. (i) Jennings, C.; Avoca, R.; Hor, A.; Loufit, R. O. *Anal. Chem.* **1984**, *56*, 2033–2035. (j) Berthod, A.; Laserna, J. J.; Winefordner, J. D. *Appl. Spectrosc.* **1987**, *41*, 1137–1141. (k) Vo-Dinh, T.; Hiromoto, M. Y. K.; Begun, G. M.; Moody, R. L. *Anal. Chem.* **1984**, *56*, 1667–1670. (l) Pal, A.; Stokes, D. L.; Alarie, J. P.; Vo-Dinh, T. *Anal. Chem.* **1995**, *67*, 3154–3159.

(16) Knill, C. J.; Kennedy, J. F.; Mistry, J.; Miraftab, M.; Smart, G.; Groocock, M. R.; Williams, H. J. *Carbohydr. Polym.* **2004**, *55*, 65–76.

(17) Annan, N. T.; Borza, A. D.; Truelstrup, L. H. *Food Res. Int.* **2008**, *41*, 184–193.

(18) Esumi, K.; Suzuki, A.; Usui, K.; Torigoe, K. *Langmuir* **1998**, *14*, 3157–3159.

(19) Pal, A.; Stokes, D. L.; Vo-Dinh, T. *Curr. Sci.* **2004**, *87*, 486–491.

(20) Kundu, S.; Pal, A.; Ghosh, S. K.; Nath, S.; Panigrahi, S.; Praharaj, S.; Pal, T. *Inorg. Chem.* **2004**, *43*, 5489–5491.

(21) Esumi, K.; Suzuki, A.; Hosoya, T.; Akihiro, N.; Torigoe, K. *J. Colloid Interface Sci.* **2000**, *226*, 346–352.

(22) Pal, A. *Mater. Lett.* **2004**, *58*, 529–534.

(23) Pal, A. *Talanta* **1998**, *74*, 14–19.

(24) Zhu, J.; Konya, Z.; Puntes, V. F.; Kiricsi, I.; Miao, C. X.; Ager, J. W.; Alivisatos, A. P.; Somorjai, G. A. *Langmuir* **2003**, *19*, 4396–4401.

(25) Shankar, S. S.; Rai, A.; Ahmad, A.; Sastry, M. *J. Colloid Interface Sci.* **2004**, *275*, 496–502.

(26) Schneider, S.; Grau, H.; Halbig, P.; Freunscht, P.; Nickel, U. *J. Raman Spectrosc.* **1996**, *27*, 57–68.

(27) Nie, S.; Emory, S. R. *Science* **1997**, *275*, 1102–1106.

(28) Mandal, M.; Jana, N. R.; Kundu, S.; Ghosh, S. K.; Panigrahi, M.; Pal, T. *J. Nanoparticle Res.* **2004**, *6*, 53–61.

(29) Muniz-Miranda, M. *J. Phys. Chem. A* **2000**, *104*, 7803–7810.

(30) Peng, Y.; Niu, Z.; Huang, W.; Shu, C.; Li, Z. *J. Phys. Chem. B* **2005**, *109*, 10880–10885.

(31) Zou, X.; Dong, S. *J. Phys. Chem. B* **2006**, *110*, 21545–21550.

(32) (a) Nikoobakht, B.; El-Sayed, M. A. *J. Phys. Chem. A* **2003**, *107*, 3372–3378. (b) Jang, N. H.; Suh, J. S.; Moskovits, M. *J. Phys. Chem. B.* **1997**, *101*, 8279–8285.

(33) (a) Sinfelt, J. H. *Bimetallic Catalyst: Discoveries Concepts and Applications*; John Wiley & Sons: New York, 1983. (b) Toshima, N.; Yonezawa, T.; Harada, M.; Asakura, K.; Iwasawa, Y. *Chem. Lett.* **1990**, 815–818.

(34) (a) Sarkar, S.; Pande, S.; Jana, S.; Sinha, A. K.; Pradhan, M.; Basu, M.; Chowdhury, J.; Pal, T. *J. Phys. Chem. C* **2008**, *112*, 17862–17876. (b) Alvarez-Puebla, R. A.; Arceo, E.; Goulet, P. J. G.; Garrido, J. J.; Aroca, R. F. *J. Phy. Chem. B.* **2005**, *109*, 3787–3792.

(35) Basu, S.; Pande, S.; Jana, S.; Bolisetty, S.; Pal, T. *Langmuir* **2008**, *24*, 5562–5568.

(36) (a) Le Ru, E. C.; Blackie, E.; Etchegoin, P. G. *J. Phys. Chem. C* **2007**, *111*, 13794–13803. (b) Cañamares, M. V.; Garcia-Ramos, J. V.; Sanchez-Cortes, S.; Castillejo, M.; Oujja, M. *J. Colloid Interface Sci.* **2008**, *326*, 103–109.

JP811235M